

Nanometer surface gratings on Si(100) characterized by x-ray scattering under grazing incidence and atomic force microscopy

T. H. Metzger,^{a)} K. Haj-Yahya, J. Peisl, M. Wendel, H. Lorenz, and J. P. Kotthaus
Sektion Physik, Ludwig-Maximilians-Universität München, Geschwister-Scholl-Platz 1, 80539 München, Germany

G. S. Cargill III
Columbia University, New York, New York 10027

(Received 22 April 1996; accepted for publication 15 October 1996)

During rapid melting and resolidification of As-implanted Si(100) by pulsed laser irradiation a periodic lateral grating has been created on the Si surface. Structure and perfection of the grating is investigated by specular and diffuse x-ray scattering under grazing incidence and exit angles. Using synchrotron radiation we find sharp, off-specular diffraction rods perpendicular to the sample surface. Their lateral separation is given by the periodicity of the grating (522 ± 1 nm), which is nearly the same as the light wavelength (530 nm) used in laser annealing the samples. Intensity measurements along the diffraction rods are used to determine the detailed structure of the surface grating by fitting the experimental results with model calculations. A sinusoidal shape is found with an average amplitude of 6 ± 1 nm. This structure is confirmed by atomic force microscopy studies. The x-ray method presented will be a unique tool also applicable in the case of buried lateral nanostructures which are not accessible by surface-sensitive techniques, e.g., scanning probe methods. © 1997 American Institute of Physics. [S0021-8979(97)05002-0]

I. INTRODUCTION

The fabrication of periodic lateral nanostructures on semiconductor surfaces is a field of high scientific interest since low-dimensional electron systems defined by these structures, such as quantum wires or quantum dots, are intended to have distinct properties compared to the 2D electron gas in semiconductor quantum-well systems.¹ Typically they are produced by a combination of lithography and pattern transfer techniques.² Recently, it has been reported that lateral structures may also be induced in such systems by pulsed laser transient thermal gratings.^{3,4} In this case the resulting structures are expected to be located in the near-surface region, while the surface itself remains unstructured. In the case of technologically relevant $\langle 100 \rangle$ Si surface, lateral nanostructures have been investigated in transport and infrared experiments.^{5,6} Etched nanometer gratings on Si surfaces are also used as well-defined substrates to study the replication properties of the nanostructures after they have been covered by other materials.⁷ Again these gratings have been fabricated by lithography and etching. It has been reported that similar structures can also be produced by laser interference patterns on semiconductor surfaces⁸⁻¹⁰ with a lateral periodicity close to the laser wavelength used.

In the present work we report on the characterization of laser-induced periodic gratings on the Si(100) surface. We have partly adopted the x-ray scattering method used by Tolán *et al.*¹¹ The off-specular diffuse scattering at grazing incidence and exit angles shows intensity streaks (so-called truncation rods) running parallel to the specular path in reciprocal space. It has been demonstrated that the coherence length necessary to obtain diffraction from such extended structures is sufficiently large for x rays from a synchrotron,

especially in case of the present scattering geometry.¹²

The grating on Si $\langle 100 \rangle$ investigated in this work has similar lateral periodicity as for the above-mentioned cases (several hundred nanometers) but much smaller heights of only some nm, with microscopic surface roughness superimposed. These structures have been produced (unintentionally) during rapid thermal annealing of Si after As implantation using a pulsed laser beam scanning over the sample surface. We do not want to speculate on the detailed mechanism that causes the evolving surface pattern, it being likely a parasitic interference effect, but rather concentrate on demonstrating how the specific x-ray method applied here can be used to characterize such a periodic perturbation of the surface. We compare the resulting structure with atomic force microscope (AFM) measurements, which are only applicable with high sensitivity if the gratings are not buried under a cap layer.

II. EXPERIMENTS

A. Sample preparation

Si(100) wafers, polished to industrial standard (surface roughness about 1 nm), have been implanted by 100 keV As ions to a dose of 6×10^{16} cm⁻² at room temperature. Recrystallization of the damaged near-surface layer has been performed by laser annealing using a Q-switched frequency-doubled Nd:YAG laser ($\lambda = 530$ nm). The laser beam has been defocused to a diameter of about 50 μ m resulting in a surface energy density of 2.2 J/cm². The sample surface was scanned in near normal incidence with a raster of partially overlapping patches. The electrical activation process thereby obtained and the corresponding structure of the As atoms in the Si matrix has been reported elsewhere together with the details of the sample preparation.¹³ Further long time furnace annealing of these samples led to electrical deactivation and a new defect complex.¹⁴ It is the aim of a

^{a)}Electronic mail: thmetzger@lrz.uni-muenchen.de

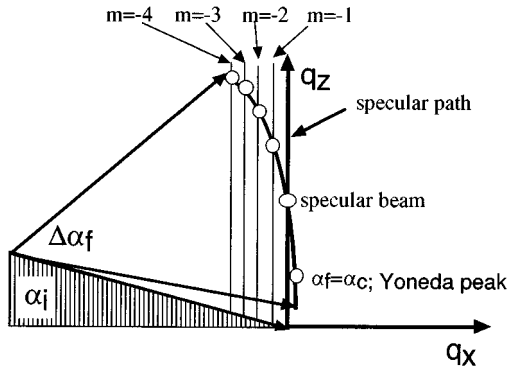


FIG. 1. Scattering geometry in the plane of incidence. Expected intensity rods $m = -1$ to -4 for a lateral grating are indicated schematically. Besides the Yoneda peak and the strong specular beam, different orders m of diffraction rods appear. The solid curve in this schematic scattering geometry at small, fixed incident angle α_i represents an exit angle scan as recorded by a position sensitive detector along $\Delta\alpha_f$.

current investigation by x-ray techniques under grazing incidence conditions to study the lattice structure and precipitations evolving in the long time annealed samples.¹⁵

Here we are interested in the surface grating that has evolved in all samples during laser annealing. Due to the high energy density and the parasitic interference of the laser beam, the local temperatures probably exceeded the melting point of Si, thus resulting in stripelike evaporation patterns on the Si surface. The presence of the high As concentration in the near-surface region may have favored this process since it is known that foreign atoms increase the absorption of laser light.⁹

B. X-ray scattering

In order to characterize a surface grating with a periodicity of some hundred nm, extremely high resolution for lateral momentum transfer is mandatory. This can only be achieved by triple crystal diffractometry¹⁶ or by choosing the scattering geometry of grazing incidence.¹² Let us assume q_x and q_z , the momentum transfer parallel and perpendicular to the sample surface, be placed in the plane of incidence. In the case of specular reflectivity the angle of incidence α_i and exit α_f are the same. Information on the density profile perpendicular to the surface is obtained. If the grating is oriented perpendicular to the incident x-ray beam, diffraction maxima at $\delta q_x = n * 2\pi/d$ are expected, where d is the periodicity of the grating. Since the grating is confined to the sample surface the diffraction maxima are extended along q_z , perpendicular to the sample surface. Figure 1 shows the scattering geometry together with the expected intensity distribution in reciprocal space. $\Delta\alpha_f$ represents the range of the exit angles covered by a position-sensitive detector (PSD). The different orders of the diffraction rods $m = -1$ through $m = -4$ are expected to appear parallel to the specular path.

The experiments have been performed using a 60 kW Rigaku rotating anode x-ray generator (Cu $K\alpha_1$ radiation) and the positron storage ring DORIS, at Hasylab, DESY, in Hamburg at the diffractometer located at beamline D4. The x-ray wavelength $\lambda = 0.13$ nm was selected by a flat Ge(111)

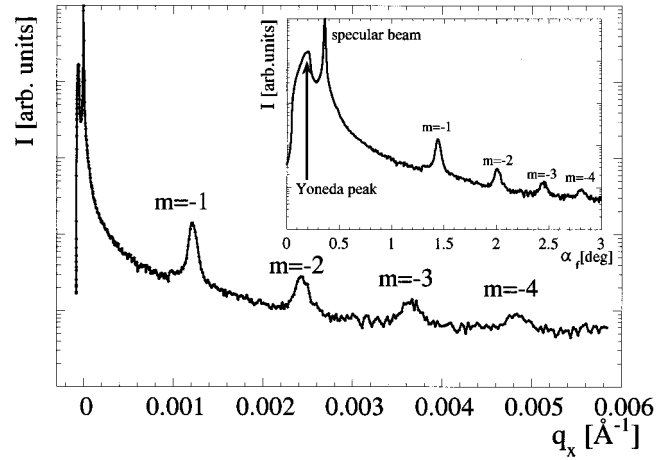


FIG. 2. Scattering intensity on a logarithmic scale as a function of the exit angle α_f at the incident angle $\alpha_i = 0.36^\circ$ (inset). The horizontal axes from the inset are converted to lateral momentum transfer q_x in the main plot. The diffraction maxima $m = -1$ to $m = -4$ become equidistant. Note that their widths are larger than the width of the specular beam.

monochromator crystal from the synchrotron beam after passing a gold mirror which suppressed the higher harmonics from the monochromator. The size of the incident beam was defined by a horizontal slit of 1 mm and a vertical slit of 0.1 mm. Details of the setup have been described elsewhere.¹² The scattered intensity was recorded by a PSD that can be rotated around an axis perpendicular to the plane of incidence. It covers an exit angle range of about 3° with a resolution of about 0.8 mrad.

In the inset of Fig. 2 the existence of diffraction rods is demonstrated by a detector ‘‘scan’’ as measured by the position sensitive detector. Cu $K\alpha_1$ radiation was used. The incident angle was kept constant at $\alpha_i = 0.36^\circ$. If the exit angle equals the critical angle for total reflection, $\alpha_f = \alpha_c$, the diffuse intensity is amplified by the transmission function (so-called Yoneda peak). For $\alpha_i = \alpha_f$ strong specular reflection is obtained, while for exit angles larger than α_i four maxima appear. They are due to different orders of Bragg diffraction, $m = -1$ to $m = -4$, from the surface grating as indicated schematically in Fig. 1. The scattering angles α_i and α_f have been converted in the vector for momentum transfer using

$$\mathbf{q} = (q_x, 0, q_z) = 2\pi/\lambda (\cos \alpha_f - \cos \alpha_i, 0, \sin \alpha_f + \sin \alpha_i).$$

Plotting the scattering intensity as a function of q_x (Fig. 2), we find the lateral distances between all diffraction rods to be constant. This distance corresponds to a mean lateral periodicity of the grating of 522 ± 1 nm.

The orientation of the grating with respect to the plane of incidence has been checked by maximizing the distance of the Bragg rods, $\delta q_x = n * 2\pi/d_{\text{eff}}$, as a function of the azimuthal angle ω , which changes the effective periodicity according to $d_{\text{eff}} = d/\sin \omega$. For $\omega = \omega_{\text{max}} = 90^\circ$ the grating is placed perpendicular to the incident beam. ω_{max} can be determined to an accuracy of 0.1° . Inspection of Fig. 2 shows that the width of the specular beam is smaller than for the satellite peaks $m = -1$ to -4 . From the full width at half-maximum (FWHM) of the first side peak the number of pe-

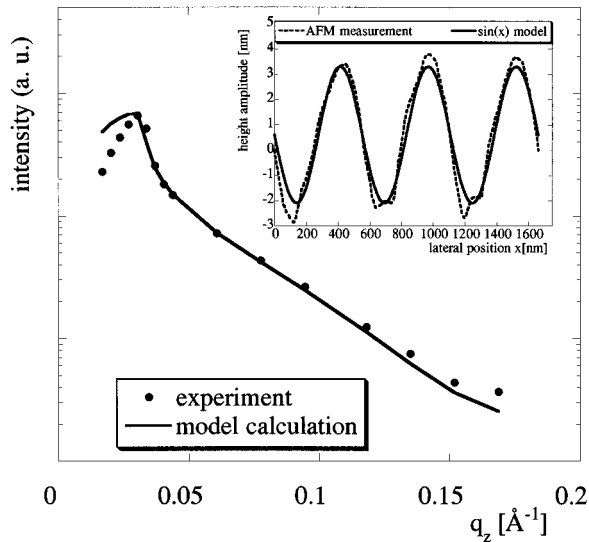


FIG. 3. Scattering intensity along the first satellite diffraction rod $m = -1$ as a function of vertical momentum transfer q_z . Circles represent the experiment, the solid line a calculation using a sinusoidal model. The inset shows the result of the model calculation (solid line) and the surface profile as obtained from AFM measurements.

riods N contributing coherently to the interference maximum is determined according to the Laue equation

$$\sin^2[N\delta q_x(d/2)]/\sin^2[\delta q_x(d/2)] = 0.5N^2.$$

$N = 13$ is obtained from this analysis and represents a real structure effect rather than the limitation by the coherence length of the x rays. The coherently eliminated length resulting from the projection of the longitudinal coherence length on the surface reaches about $300 \mu\text{m}$.¹² The grating imperfection is presumably due to the perturbation of the long-ranged periodicity created by the laser-induced lateral structuring mechanism. This perturbation will become obvious by the AFM measurements taken at different locations on the sample surface (see below).

C. Quantitative interpretation

In the following the detailed structure of the surface grating is characterized by comparing further x-ray measurements with model calculations for the off-specular structure factor of a periodic surface “roughness” using the theory outlined recently by Tolan *et al.*¹¹ They have shown that the real structure of a surface grating can be obtained by measuring the q_z dependence of both the specular reflectivity and the satellite diffraction rods. To do so, we have performed a q_z scan along the first two diffraction maxima, by varying α_i and the PSD in a manner that kept the specular peak always at the same channel number in the multichannel analyzer which records the PSD signal. For intensity reasons this measurement was done using synchrotron radiation. The background corrected integrated intensity of the first diffraction satellite peak, $m = -1$, is shown as a function of momentum transfer q_z in Fig. 3 at constant $q_x = 2\pi/d$. The circles represent the measurement, while the solid line shows results of a model calculation, which is explained later. Qualita-

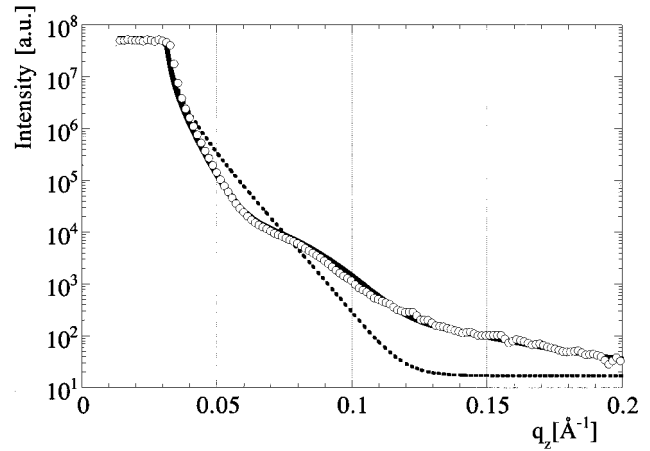


FIG. 4. Specular intensity ($m=0$) as a function of perpendicular momentum transfer q_z . Open circles represent the experimental data, the dashed line is a calculation using a Gaussian surface roughness of 2.3 nm. The solid line shows the result of a fit for which the surface grating has been replaced by a sinusoidal surface layer with an average thickness of 6 nm.

tively this measurement can be interpreted as follows: The intensity maximum is again caused by the transmission function at $\alpha_i = \alpha_c$ and is followed by a structureless monotonic intensity decay along q_z . The absence of further intensity oscillations for $\alpha_i > \alpha_c$ indicates that the grating height is much smaller than its periodicity. For other systems with larger grating heights pronounced oscillations have been found.^{11,16} From the following evaluation it becomes clear that the amplitude of the surface grating is still too large to be treated as a small perturbation of the surface and thus can not be described by a Gaussian roughness. In addition the spectral power density of the grating is quite different from a surface with a self-affine height–height correlation function. This difference is now demonstrated from the analysis of the specular reflectivity ($m=0$) as shown in Fig. 4. Again the grating is oriented perpendicular to the incident beam. The Fresnel decay of the specular intensity is modulated by a weak intensity oscillation. Using a simulation program for specular reflectivity of layered flat samples (REFSIM by Siemens) the experimental data have been fitted by two models. First, a flat surface with Gaussian roughness of 2.3 nm has been assumed. The corresponding curve in Fig. 4 clearly does not reproduce the experimental data. Second, the grating is modeled by a layer with sinusoidal vertical amplitudes $z = h^* \sin(x/d)$ on top of the Si substrate with an average density smaller than Si bulk density. The corresponding calculated specular reflectivity is shown in Fig. 4 as a solid line. Due to the crude assumptions made in the model the only reliable parameter in the fit is the layer thickness of $2h = 6 \pm 1$ nm. It determines the location of the intensity modulation around $q_z = 0.09 (\text{\AA}^{-1})$. We conclude that the specular reflectivity measurement is able to distinguish between Gaussian and structured roughness even for relatively small height. For the remainder of this subsection we want to determine the detailed structural parameter of the grating from model calculations using the theory reported by Tolan *et al.*¹¹ in the kinematic approximation. Two models have been compared: a sinusoidal grating profile and a periodic grating with an

asymmetric trapezoidal shape. The simulation resulting from the sinusoidal shaped grating is represented by a solid line in Fig. 3 and fits the data reasonably well. The disagreement between the fitted and experimental curve for α_i smaller than the critical angle is caused by a trivial geometric effect, which contains no further structural information. The structure obtained by the fitting is compared to the grating profile measured directly by AFM (see inset of Fig. 3). The main result from the fitting is the average grating height: $2h=6\pm 1$ nm has been found. The model calculation is rather insensitive to the periodicity of the grating. We therefore used the periodicity $d=540\pm 30$ nm as obtained from averaging several AFM measurements. Within this error bar the model calculations produced fits similar to the one given in Fig. 3.

The trapezoidal model fits the measured data with similar quality (not shown in Fig. 3) but the amplitude of the grating is too small by a factor of about 2 as compared to the AFM result.

D. AFM measurement

Finally, we present the result of AFM measurements which probe the surface grating in real space. They have been performed with a NANOSCOPE III in the tapping mode. In this mode the cantilever vibrates at its resonance frequency of about 300 kHz, resulting in an amplitude to the order of 10 nm. To obtain high topographic resolution we fabricated needlelike, electron-beam-deposited supertips with a typical tip length of $1\ \mu\text{m}$ and a tip diameter of about 100 nm. Some of these tips were additionally sharpened in an oxygen plasma, resulting in a decrease of the tip diameter by a factor of 3–4. For a detailed description of the tip fabrication we refer to Ref. 17. An area up to $14\times 14\ \mu\text{m}^2$ has typically been scanned in the AFM measurement. The resulting topography is shown in the lower part of Fig. 5, while in the upper part the vertical section plot along the line A, B is presented. The average periodicity of the grating is 522 nm, the amplitude in this section varies from 3 to 5 nm. Taking several such pictures at different locations on the sample surface we find that the grating is far from being perfect. It shows varying amplitudes between 2 and 10 nm and periodicities between 510 and 570 nm (540 ± 30 nm). Typical length scales over which the grating is reasonably perfect amount to 4000–7000 nm. The number of periods within such a length ranges from $N=8$ to $N=14$ and gives a similar value as obtained from the FWHM of the x-ray satellite rods ($N=13$). An amplified section of one of the surface profiles obtained by AFM measurements is compared to the result from x-ray scattering in the inset of Fig. 3.

III. DISCUSSION AND CONCLUSION

The structure of a laser-induced lateral grating on Si(100) is determined in detail by x-ray scattering at grazing incidence and exit angles and in real space by AFM. Keeping in mind that the averaging in x-ray scattering is performed over macroscopic dimensions while the high-resolution AFM measurement images only some μm , we conclude that the results of both methods agree reasonably well. In the present scattering geometry the x-ray coherence length pro-

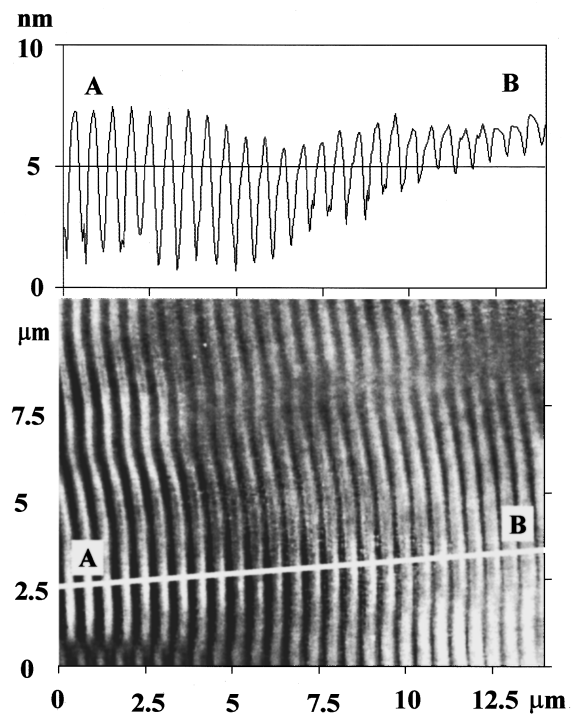


FIG. 5. AFM topography of the surface grating (lower part). Surface profile along the section A, B (upper part). Periodicity of 522 nm and height amplitudes between 3 and 5 nm are found.

jected on the sample surface is enlarged by a factor of more than 100 and the resolution for lateral momentum transfer becomes as high as $1.5\times 10^{-5}\ \text{\AA}^{-1}$.¹² Thus, lateral periodic patterns with a periodicity of up to $10\ \mu\text{m}$ can be investigated by x rays. The lower limit of such structures is of course determined by the atomic distances which are still far from being realized by current lateral patterning techniques.

We finally want to emphasize that the comparison between the two methods will not be possible in the case of buried gratings; then diffuse x-ray scattering will be the unique tool to characterize such structures. In addition to the characterization of periodic lateral electron density modulations as demonstrated by the x-ray methods presented here, diffraction under grazing incidence from such buried structures will show how the corresponding atomic order is changed by the lateral patterning of crystalline samples.

First measurements on buried lateral gratings in GaAs/AlGaAs heterostructures revealed encouraging results.¹⁸

ACKNOWLEDGMENTS

We want to thank H. Rhan and G. Goerigk for valuable help during our stay at HASYLAB. One of us (K.H.) wants to thank the DAAD for financial support and M. Tolan for fruitful discussions. Enlightening conversations with T. Salditt are gratefully acknowledged. We are grateful for financial support from BMFT under Grant No. 055MAXI5 and from Volkswagen-Stiftung I/68769.

¹W. Hansen, J. P. Kotthaus, and U. Merkt, in *Semiconductor and Semimetals*, edited by R. K. Willardson, A. C. Beer, and E. R. Weber (Academic, San Diego, 1992), Vol. 35, p. 279.

- ²H. G. Craighead, in *Physics of Nanostructures*, edited by J. H. Davies and A. R. Long (IOP, London, 1992), p. 21.
- ³K. F. Brunner, Ph.D. thesis, Walter Schottky Institut der Technischen Universität München, 1993.
- ⁴M. Heintze, P. V. Santos, C. E. Nebel, and M. Stutzmann, *Appl. Phys. Lett.* **64**, 1 (1994); M. K. Kelly, C. E. Nebel, M. Stutzmann, and G. Böhm, *ibid.* **68**, 1984 (1995).
- ⁵P. F. Bagwell, S. L. Park, A. Yen, D. A. Antoniadis, H. J. Smith, and T. P. Orlando, *Phys. Rev. B* **45**, 9214 (1992).
- ⁶A. Huber, H. Lorenz, J. P. Kotthaus, S. Bakker, and T. M. Klapwijk, *Phys. Rev. B* **51**, 5028 (1995).
- ⁷M. Tolan, G. Vacca, S. K. Sinha, Z. Li, M. Rafailovich, J. Sokolov, H. Lorenz, and J. P. Kotthaus, *J. Phys. D* **28**, A231 (1995).
- ⁸J. S. Preston, H. M. van Driel, and J. E. Sipe, *Phys. Rev. Lett.* **58**, 69 (1987).
- ⁹M. Wittmer and G. A. Rozgonyi, in *Current Topics in Material Science*, edited by E. Kaldis (North-Holland, Amsterdam, 1982), Vol. 8, Chap. 1.
- ¹⁰J. E. Sipe, J. F. Young, J. S. Preston, and H. M. van Driel, *Phys. Rev. B* **27**, 1141 (1983); J. F. Young, J. S. Preston, H. M. van Driel, and J. E. Sipe, *ibid.* **27**, 1155 (1983).
- ¹¹M. Tolan, W. Press, F. Brinkop, and J. P. Kotthaus, *Phys. Rev. B* **51**, 2239 (1995).
- ¹²T. Salditt, H. Rhan, T. H. Metzger, H. Peisl, J. Schuster, and J. P. Kotthaus, *Z. Phys. B* **96**, 227 (1994).
- ¹³J. M. Tonnerre, M. Matsuura, G. S. Cargill III, and L. W. Hobbs, *Mater. Res. Soc. Symp. Proc.* **209**, 505 (1991); A. Erbil, W. Weber, G. S. Cargill III, and R. F. Boehme, *Phys. Rev. B* **34**, 1392 (1986).
- ¹⁴K. C. Pandey, A. Erbil, G. S. Cargill III, R. F. Boehme, and D. Vanderbilt, *Phys. Rev. Lett.* **61**, 1282 (1988).
- ¹⁵K. Haj-Yahya, T. H. Metzger, and J. Peisl (unpublished).
- ¹⁶M. Tolan, W. Press, F. Brinkop, and J. P. Kotthaus, *J. Appl. Phys.* **75**, 7761 (1994).
- ¹⁷M. Wendel, H. Lorenz, and J. P. Kotthaus, *Appl. Phys. Lett.* **67**, 3732 (1995).
- ¹⁸T. H. Metzger, C. E. Nebel, M. K. Kelly, M. Stutzmann, and J. Peisl (unpublished).